PHYSICAL REVIEW B VOLUME 47, NUMBER 16 15 APRIL 1993-II

Determination of (1×1) and (1×2) structures of Pt thin films on Pd(110) by dynamical low-energy electron-diffraction analysis

O. L. Warren, H.-C. Kang,* P. J. Schmitz,† and P. A. Thiel
Department of Chemistry and Ames Laboratory, Iowa State University, Ames, Iowa 50011

P. Kaukasoina and M. Lindroos
Tampere University of Technology, P.O. Box 527, SF-33101, Tampere, Finland

(Received 29 May 1992; revised manuscript received 13 January 1993)

Geometric structures of (1×1) and (1×2) Pt thin films on Pd(110) have been determined by dynamical low-energy electron-diffraction analysis. The (1×1) structure is found to exhibit relaxations in the first two interlayer spacings of $\Delta d_{12}=-11.0\%$ and $\Delta d_{23}=6.6\%$ at a Pt coverage of one monolayer, and relaxations of $\Delta d_{12}=-6.6\%$ and $\Delta d_{23}=4.4\%$ at two monolayers. As for the (1×2) structure, the top three layers are found to be Pt. The topmost layer is of the missing-row type, the second layer is slightly row paired (0.06 Å), and the third layer is significantly rumpled (0.23 Å). Relaxations in the first four interlayer spacings are found to be $\Delta d_{12}=-9.5\%$, $\Delta d_{23}=-8.0\%$, $\Delta d_{34}=-7.3\%$, and $\Delta d_{45}=2.2\%$. Except for a significantly less contracted first interlayer spacing, the (1×2) structure of the Pt film mimics the (1×2) structure of bulk Pt(110).

I. INTRODUCTION

The (110) face of bulk Pt is known to reconstruct. The two most commonly observed periodicities—(1×2) and (1×3)— have been shown to correspond to geometries of the missing-row type.[1-3] However, the clean surface of Pd(110) is known to be stable with respect to reconstruction.[4-6] Thus, a Pt film on Pd(110) represents a reconstructive film grown atop a nonreconstructive substrate. Since the lattice mismatch is only 0.8%,[7] one would not expect this factor to play a major role in determining the film structure or growth mode, at least for the first few layers.[8]

Recently, we have observed (1×1), (1×2), and (1×3) low-energy electron diffraction (LEED) patterns for Pt thin films grown on Pd(110).[9,10] Conditions required to produce each LEED pattern are as follows. [A Pt coverage of one monolayer (ML) is defined as the atomic density of the Pd(110) surface.] For Pt coverages ≤ 1 ML, only a (1×1) LEED pattern is observed. A (1×1) LEED pattern is also observed for Pt coverages greater than 1 ML, but only if the films are deposited and maintained at low temperature. Upon annealing, these films exhibit a streaky LEED pattern for Pt coverages between 1 and 2 ML, and either a (1×2) or a (1×3) LEED pattern for Pt coverages ≥ 2 ML. All films are unstable with respect to extensive dissolution if annealed to a sufficiently high temperature,[9,10] which is consistent with the fact that Pt and Pd are known to be continuously miscible in the solid state.[11]

Interestingly, two specific conditions must be met to produce the (1×2) structure. First, the (1×2) structure develops only at 2 ML; slightly lower coverages result in no distinct superstructure and slightly higher coverages result in the (1×3) structure. Second, the formation of the (1×2) structure at 2 ML requires that Pt be deposited at temperatures less than 200 K; higher deposition temperatures result in the (1×3) structure. This is particularly surprising since relatively high annealing temperatures are required to form either superstructure. We have investigated the possibility that the peculiarity at 2 ML is the result of temperature-dependent contamination,[9] but have concluded that this is unlikely; furthermore, one would expect contamination to exert a similar effect at higher coverages. Therefore, we believe that the peculiarity is caused instead by a strong temperature dependence in the morphology of the film prior to annealing.

The similarity between the periodicities observed for the (110) face of bulk Pt and those we observe here suggests that the two systems share a common origin, i.e., the (1×2) and (1×3) structures of the Pt films are reconstructions of the missing-row type. This hypothesis is supported by the fact that exposing either the (1×2) or the (1×3) structure of the Pt films to CO "lifts" the reconstruction,[9,10] which is also known to occur on the corresponding bulk Pt surfaces.[3,12]

In this paper, we present the results of a dynamical LEED study, in which we have investigated the (1×1) structure at 1 ML, the (1×1) structure at 2 ML, and the (1×2) structure of Pt on Pd(110). While LEED has been used extensively in obtaining detailed structural information for clean and absorbate-induced reconstructions of bulk fcc(110) surfaces, here we report on a structural determination by LEED for a reconstructed fcc(110) thin film.

II. EXPERIMENTAL PROCEDURES

Experiments are performed in a stainless-steel ultrahigh-vacuum chamber (base pressure $\leq 1\times10^{-10}$ torr) equipped with a single-pass cylindrical mirror analyzer for Auger electron spectroscopy (AES); quadrupole mass spectrometer; μ-metal-shielded, display-type, four-grid LEED optics; sputter gun; provisions for gas exposure; and metal evaporator for Pt deposition. The Pd(110) crystal is cleaned by cycles of Ar^+ bombardment at 300 K and annealing at 1100 K until impurities, with the exception of carbon, are reduced to the noise level of AES. Since carbon levels are difficult to ascertain by AES due to the overlap of the carbon 272-eV and Pd 279-eV Auger signals, cycles of oxygen exposure at 640 K to remove carbon as carbon oxides and flashes to 1100 K to desorb residual oxygen are performed. Carbon levels are considered to be sufficiently low when thermal desorption spectra for the CO-saturated surface are consistent with those previously reported for a carbon-free surface.[13] Cleaning in the above manner results in a surface that exhibits a high quality (1×1) LEED pattern.

Pt is deposited at 105 K, at a rate of ca. 1 ML $\min^{-1}$. After deposition, the LEED pattern is (1×1) and no impurities are detected by AES. Relative Pt coverage is determined by measuring $R_{\mathrm{Pt/Pd}}$, which is defined as the ratio of the peak-to-peak Auger signals for Pt (64 eV) and Pd (330 eV); 2-keV primary beam energy and 1-V peak-to-peak modulation voltage are used in AES work. Measurements of $R_{\mathrm{Pt/Pd}}$ at various sample positions indicate that the films are spatially uniform to within $\pm5\%$. Figure 1 shows that linear segments and equidistant breaks characteristic of layer-by-layer growth[14] are observed in a plot of the Pt 64-eV peak-to-peak height versus cumulative deposition time. Values obtained for $R_{\mathrm{Pt/Pd}}$ at the first (0.30) and second (0.75) break points, or at 1 and 2 ML, are found to be in excellent agreement with those reported previously for the first two monolayers of Pt on Pd(100) based on the characterization of coverage-dependent Bragg intensity oscillations.[15]

The (1×1) films are not annealed to ensure that only the (1×1) phase is present. LEED patterns for 1- and 2-ML films are not as good as that of the clean substrate, but are of sufficient quality to acquire reliable intensity-energy $[I(E)]$ curves, i.e., no serious loss of low-intensity features is observed. Of the two, the LEED pattern for the 2-ML film is worse due to slightly higher background intensity and visibly detectable oscillations in spot size with beam energy. Although still visible, LEED patterns at higher coverages are degraded to the extent that an analysis is not warranted.

The (1×2) structure is produced by annealing the 2-ML film at 530 K. This procedure results in a bright, low-background LEED pattern with comparable integral and half-order intensities, although as shown in Fig. 2, half-order beams remain rather broad along the [001] direction. Neither impurities nor loss of Pt are detected by AES after annealing.

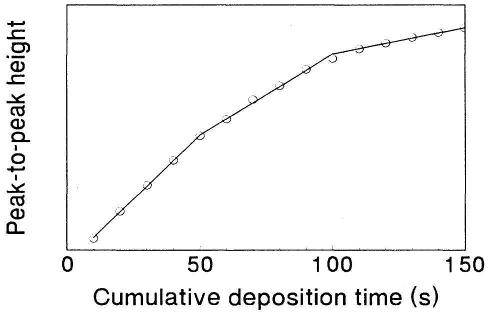

FIG. 1. Peak-to-peak height of the Pt 64-eV AES signal vs cumulative deposition time. Deposition and AES measurements are performed at 105 K.

Experimental $I(E)$ curves are acquired at normal incidence with a computer-interfaced video processor and a silicon-intensified-target camera. The crystal is maintained at 105 K. Background subtraction is performed locally during data collection, and beam-current normalization is performed separately by measuring the current as a function of energy with the crystal biased sufficiently positive to suppress secondary emission. Equivalent beam averaging—a procedure known to minimize residual experimental errors[16]—is performed when possible. Eight symmetry nonequivalent curves over the energy range of 50–250 eV are available for each of the (1×1) films, and nine symmetry nonequivalent curves (five integral-order, four half-order) over the energy range of 30–300 eV are available for the (1×2) structure. Truncation of curves prior to the maximum energy is due to either manipulator shadowing or the inability to track the beam over an extended energy range of low intensity.

Normal incidence is determined by comparing symmetry-equivalent $I(E)$ curves. In particular, the (1,1) beam set of the (1×2) LEED pattern is found to be extremely sensitive to misalignment. Figure 3 shows that while curves collected at normal incidence are in excel-

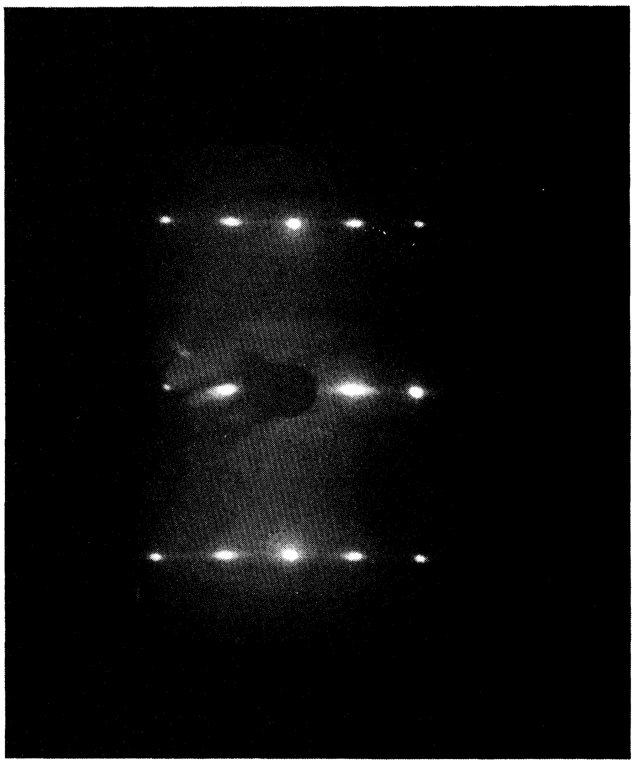

FIG. 2. (1×2) LEED pattern at 70 eV. $(0,\frac{1}{2})$, (0,1), (1,0), $(1,\frac{1}{2})$, and (1,1) beam sets are visible. Note the elongation of the half-order beams along the [001] direction.

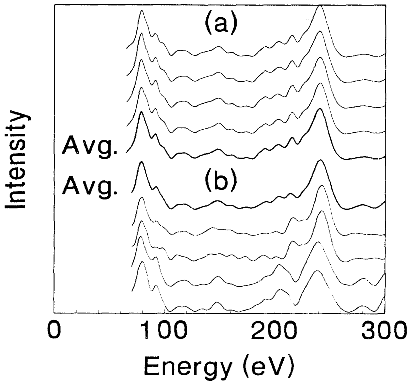

FIG. 3. (a) Experimental $I(E)$ curves for the (1,1) beam set of the (1×2) LEED pattern and their average at normal incidence. From top to bottom, beam indices are $(-1,1)$, $(-1,-1)$, $(1,-1)$, and (1,1). (b) As in (a), but for 0.5° off-normal incidence. Note the close similarity between averaged curves.

lent agreement, a small deliberate misalignment results in substantial differences. However, the merit of equivalent beam averaging is readily apparent by noting the close similarity between averaged curves.

III. COMPUTATIONAL PROCEDURES

Theoretical $I(E)$ curves are calculated with the LEED package of Van Hove and Tong.[17] After calculating reflection and transmission matrices within the self-consistent formalism, interlayer scattering is accomplished by layer doubling. The combined space method for composite layers with matrix inversion is employed when small spacings between subplanes are involved. Random substitutional disorder is studied with the average T-matrix approximation (ATA),[18] which has been shown to yield calculationally correct results.[19]

In the (1×1) analysis, eight phase shifts ($l_{\max}=7$) are used throughout. Pd phase shifts are calculated from the tabulated potential of Moruzzi, Janak, and Williams,[20] and spin-averaged Pt phase shifts are calculated from the potential of Wang.[21] The phase shifts are temperature corrected with a Debye temperature (Θ_D) of 230 K for Pd and 195 K for Pt. In the (1×2) analysis, up to nine phase shifts ($l_{\max}=8$) are included. Pd phase shifts are calculated from the potential described above, and spin-averaged Pt phase shifts are calculated from the potential of Mattheiss.[22] The phase shifts are temperature corrected with a Θ_D of 195 K for Pd and 160 K for Pt. The real part of the optical potential (V_{or}) is treated as a constant over the entire energy range, and is shifted in 1-eV steps during r-factor analysis to obtain the best level of agreement. The final value of V_{or} is -6 eV for all three structures. The imaginary part of the optical potential (V_{oi}) is fixed at -5 eV in the (1×1) analysis, and at -4 eV in the (1×2) analysis. No further steps are taken to improve the level of agreement through the values of the nonstructural parameters since such steps generally have little influence on the final structural result.[23]

Theoretical and experimental $I(E)$ curves are compared quantitatively with the Pendry r factor (r_P).[24] Since this r factor is highly sensitive to spectral noise,[24] both sets of curves are smoothed prior to r-factor analysis.

IV. (1×1) RESULTS

In the analysis of the (1×1) structures, we consider only overlayer geometries, since complications due to intermixing seem unlikely in light of the fact that the (1×1) films are deposited and maintained at low temperature. However, the number of Pt layers is considered as a variable in order to test our Pt coverage assignments based on the AES plot shown in Fig. 1. An acceptable fit between theory and experiment for both 1- and 2-ML films will confirm that a significant degree of layer-by-layer quality is indeed achieved for the first two monolayers of film growth.[25]

Results are summarized in Table I. Initially, the relaxation of the first interlayer spacing is considered for zero to three Pt layers. From the r-factor results, it is clear that 1- and 2-ML films are best described by one and two Pt layers, respectively. Optimum first interlayer spacings and minimum r factors for one-layer relaxation are as follows: $d_{12}=1.25$ Å and $r_P=0.39$ for the 1-ML film; $d_{12}=1.31$ Å and $r_P=0.35$ for the 2-ML film.

Next, the (1×1) structures are further refined by considering relaxations in the first two interlayer spacings. Optimum first and second interlayer spacings and minimum r factors for two-layer relaxation are as follows: $d_{12}=1.22$ Å, $d_{23}=1.46$ Å, and $r_P=0.27$ for the 1-ML film; $d_{12}=1.28$ Å, $d_{23}=1.43$ Å, and $r_P=0.30$ for the 2-ML film. Differences in the interlayer spacings relative to the truncated substrate geometry are as follows: $\Delta d_{12}=-11.0\%$ and $\Delta d_{23}=6.6\%$ for the 1-ML film; $\Delta d_{12}=-6.6\%$ and $\Delta d_{23}=4.4\%$ for the 2-ML film. As expected, by allowing d_{23} to expand, a further contraction in d_{12} is found for both films.[26] Based on Pendry's definition of the variance,[24] an uncertainty of ca. ±0.03 Å (±2%) is associated with each interlayer spacing. Changes in deeper interlayer spacings are not considered since they are most likely smaller than their associated uncertainties. For example, while a first-principles calculation for a single (1×1) layer of Au on Ag(110) predicts relaxations in the first two interlayer spacings comparable

TABLE I. Results of the (1×1) analysis. Dash indicates that the parameter is not varied.

ML (expt.)	Number of Pt layers (theory)	Optimum parameters (Å) z_{12}	z_{23}	Pendry r factor
1	0	1.33	—	0.61
1	1	1.25	—	0.39
1	2	1.34	—	0.52
1	3	1.36	—	0.61
2	0	1.35	—	0.61
2	1	1.38	—	0.57
2	2	1.31	—	0.35
2	3	1.32	—	0.52
1	1	1.22	1.46	0.27
2	2	1.28	1.43	0.30

to those found for the 1-ML Pt film ($\Delta d_{12}=-11.9\%$, $\Delta d_{23}=5.5\%$), it predicts only a negligible relaxation in the third interlayer spacing ($\Delta d_{34}=-0.7\%$).[27] Contour maps of r_P as a function of the first two interlayer spacings are shown in Fig. 4. Experimental and best-fit theoretical $I(E)$ curves are visually compared in Figs. 5 and 6.

Pendry r factors obtained for both films are somewhat higher than the values of <0.20 typically expected for clean surfaces of unreconstructed metals, which could be due in part to surface roughness. [Although it should be noted that such low values are generally not achieved for high-Z metals such as Pt, e.g., a Pendry r factor of only 0.50 was reported for the clean surface of Pt(111)-(1×1).[28]] As mentioned previously, LEED patterns for both films are poorer than that of the clean substrate, and oscillations in spot size with beam energy are detected in the case of the 2-ML film, which indicates the presence of random steps.[29] The presence of steps has been previously implicated as a cause for degrading the level of agreement in LEED analysis.[30] Despite the apparent deviation from ideality, the predominant ordered component of the 1- and 2-ML films is clearly shown to be one and two layers thick, respectively, which confirms that film growth at low temperature occurs in at least a pseudo-layer-by-layer fashion for the first two monolayers, i.e., the interface width is considerably narrower than predicted by Poisson statistics. This behavior has also been observed for low-temperature growth of Pt on Pd(100).[31] For statistically random deposition on an fcc(100) substrate, it has been demonstrated that diffusionless pseudo-layer-by-layer growth is feasible, with the stipulation that adsorption can occur only in fourfold hollow sites.[32] An analogous explanation may apply here.

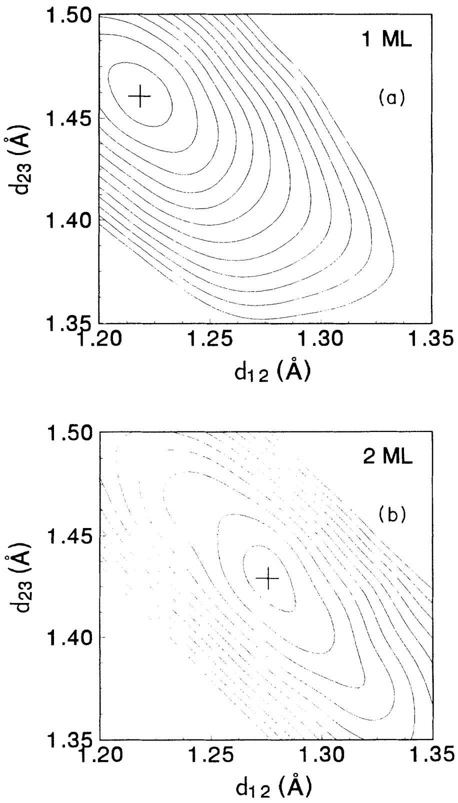

FIG. 4. Pendry r factor contour maps for the (1×1) structures. The innermost contour corresponds to $r_P=0.28$ in the 1-ML map (a), and to $r_P=0.31$ in the 2-ML map (b). Each successive contour corresponds to an increase in r_P of 0.02.

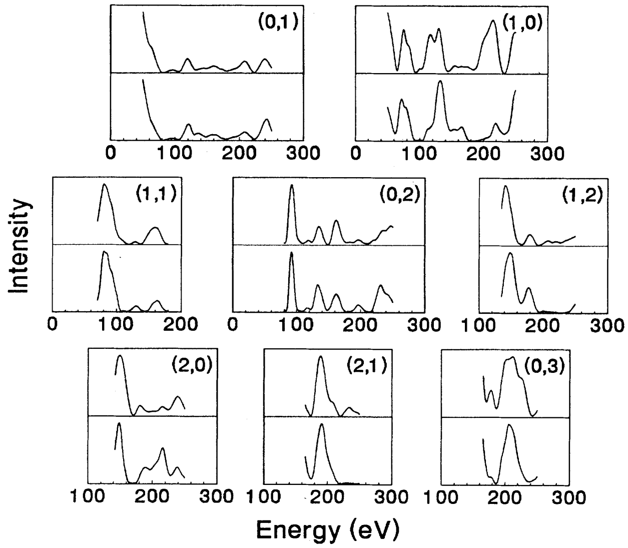

FIG. 5. Experimental and best-fit theoretical $I(E)$ curves for the (1×1) structure at 1 ML. Upper curves correspond to theory.

V. (1×2) RESULTS

In the analysis of the (1×2) structure, we focus primarily on missing-row-type models. However, paired-

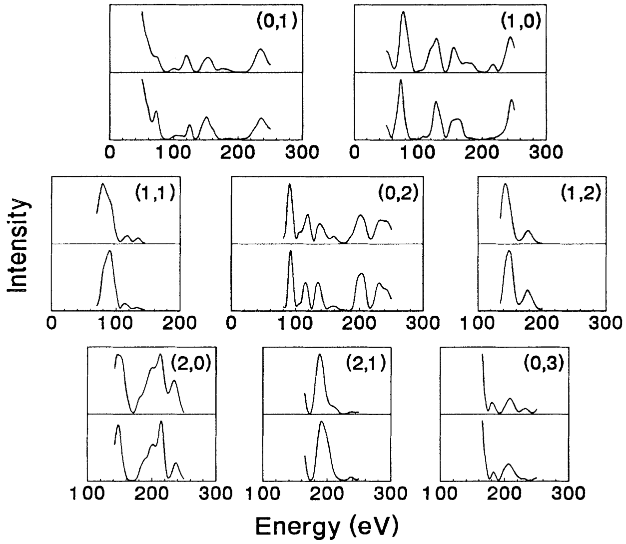

FIG. 6. Experimental and best-fit theoretical $I(E)$ curves for the (1×1) structure at 2 ML. Upper curves correspond to theory.

row, rumpled-surface, and sawtooth[33] models are also tested since the electronic influence of the Pd substrate may induce a reconstruction different from that of bulk Pt. Descriptions of these models can be found in Ref. 34. Since the ideal coverage of the (1×2) phase is not exactly known experimentally, the number of Pt layers is treated as a variable. In addition, the possibility of intermixing is considered for the (1×2) structure since its formation requires a relatively high annealing temperature. Structural parameters—interlayer spacings (d_{12}–d_{45}), extent of pairing (σ), and extent of rumpling (δ)—are defined in Fig. 7 for the missing-row model with second-layer row pairing and third-layer rumpling. These parameters are similarly defined for models not shown.

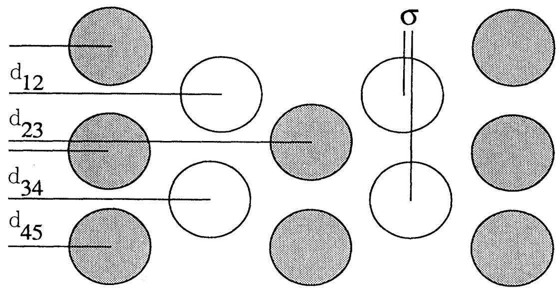

FIG. 7. Schematic of the missing-row model with second-layer row pairing and third-layer rumpling. Sign conventions for pairing (σ) and rumpling (δ) are as follows: positive pairing corresponds to pairing towards the missing row, and negative rumpling corresponds to the situation where the upper atom in the rumpled layer is directly beneath the missing row. The schematic is drawn to exhibit positive pairing and negative rumpling.

First, overlayer models are considered. Results for these models are summarized in Table II. Correctness of a missing-row topmost layer is clearly demonstrated by the r-factor results for models 1–4. The missing-row model yields the lowest r factor (0.54) when compared to paired-row (0.75), rumpled-surface (0.65), and sawtooth (0.77) models. The missing-row model is also preferred when partial r factors for integral and half-order beams are taken separately into account. Since the optimum pairing in the paired-row model corresponds to the situation with no pairing, the partial r factor for the half-order beams is estimated to be 1. Although the number of Pt layers is fixed at three at this stage of the analysis, we believe that models 2–4 can be excluded from further consideration. [A film thickness of N layers corresponds to an ideal coverage of $(N-0.5)$ ML for the missing-row model, $(N-1)$ ML for the sawtooth model, and N ML for paired-row and rumpled-surface models.]

However, the r factor for the missing-row model is still rather poor; thus, the sensitivity of LEED with respect to the number of Pt layers is tested in models 5–7. While r factors for one (0.60) and two (0.60) layers are worse, it is somewhat disturbing that the same level of agreement is achieved for zero (0.55) and three (0.54) layers. The failure to identify the number of Pt layers suggests that the missing-row model is not a complete description of the reconstruction. Although the first LEED analysis of bulk Pt(110)-(1×2) favored the missing-row model, the results were not conclusive owing to an incomplete account of the full extent of the reconstruction.[35] Subsequent LEED analyses have shown that an extension of the reconstruction to subsurface layers in the form of alternating row pairing and rumpling is necessary to obtain an acceptable fit between theory and experiment.[2,3] Thus, the missing-row model is extended to include these features, with the number of Pt layers remaining as a variable.

In models 8–12, the effect of row pairing in the second layer and rumpling in the third layer is studied for zero to four Pt layers. While r factors for zero, one, two, and four layers remain above 0.50, a significantly improved r factor (0.32) is achieved for three layers (model 11). Comparable partial r factors are obtained for integral (0.30) and half-order (0.35) beams.

TABLE II. Results for (1×2) overlayer models. Missing-row model with second-layer row pairing and third-layer rumpling is denoted as M+P+R. Missing-row model with rumpling in the second layer is denoted as M+R. Dash indicates that the parameter is either not relevant to the model under consideration or is not varied.

	Number of Pt layers	Optimum parameters (Å)						Pendry r factor		
Model	(theory)	z_{12}	z_{23}	z_{34}	z_{45}	σ	δ	Int.	Half	Tot.
1 Missing-row	3	1.27	1.59	1.21	1.40	—	—	0.47	0.64	0.54
2 Paired-row	3	1.29	1.53	1.28	1.44	0.00	—	0.52	1.00	0.75
3 Corrugated-surface	3	1.19	1.41	1.41	1.38	—	−0.16	0.52	0.79	0.65
4 Sawtooth	3	1.26	1.18	1.25	—	—	—	0.75	0.78	0.77
5 Missing-row	0	1.24	1.21	1.54	1.39	—	—	0.52	0.58	0.55
6 Missing-row	1	1.30	1.26	1.44	1.38	—	—	0.57	0.63	0.60
7 Missing-row	2	1.20	1.35	1.42	1.38	—	—	0.56	0.64	0.60
8 M+P+R	0	1.25	1.21	1.44	1.39	−0.19	−0.09	0.53	0.53	0.53
9 M+P+R	1	1.27	1.25	1.36	1.37	0.09	−0.07	0.57	0.57	0.57
10 M+P+R	2	1.19	1.32	1.35	1.36	0.08	−0.10	0.52	0.59	0.55
11 M+P+R	3	1.24	1.26	1.27	1.40	0.06	−0.23	0.30	0.35	0.32
12 M+P+R	4	1.22	1.28	1.29	1.37	−0.01	−0.23	0.58	0.45	0.52
13 M+R	3	1.26	1.58	1.21	1.40	—	−0.02	0.47	0.64	0.54

While pairing in the second layer of model 11 is found to be only slight ($\sigma = 0.06$ Å), rumpling in the third layer is found to be significant ($\delta = -0.23$ Å). It is known that vertical displacements, such as rumpling, exert a large effect on $I(E)$ curves due to momentum transfer being primarily toward the surface normal in the normal-incidence configuration.[34] By the same reasoning, $I(E)$ curves are somewhat insensitive to lateral displacements such as row pairing.[34] Thus, we conclude that the omission of third-layer rumpling is the principal cause for the above-mentioned failure to identify the number of Pt layers within the (1×2) structure. [Due to the weak effect of row pairing, a missing-row model with three Pt layers and rumpling instead of pairing in the second layer is also tested (model 13); however, the *r*-factor result for this model (0.54) indicates that this is not a good choice for the position of the rumpled layer.]

Next, intermixing models are considered. Results for these models are summarized in Table III. Random substitutional disorder within the first four layers of the missing-row model with second-layer row pairing and third-layer rumpling is studied with the ATA method in models 14–17. While the atomic concentration is varied for the layer under consideration, all structural parameters and all other layer compositions are fixed as listed for model 11 in Table II. The results favor a small amount of Pd in the topmost layer (12%), but this cannot be judged conclusive since the *r* factor obtained for no intermixing clearly falls within the range of uncertainty.

Since the rumpled layer in model 11 is in direct contact with the substrate, the possibility of a 1:1 ordered alloy in this layer is considered in models 18 and 19. However, after reoptimization of the structural parameters, we find that the *r* factor increases to 0.44 for Pt as the upper atom in the rumpled layer, and to 0.48 for Pd as the upper atom in the rumpled layer. A preference for Pt rather than Pd as the upper atom is a further indication that this layer is all Pt.

Finally, combinations of missing-row Pt or (Pd+Pt) in the topmost layer; 2Pt, (Pd+Pt), or (Pt+Pd) in the second and third layers; and 2Pd, (Pd+Pt), or (Pt+Pd) in the fourth layer are tested (results are not listed in Table III owing to the large number of combinations). The first four interlayer spacings are taken into account, but neither pairing nor rumpling is considered. In all cases, at least the mirror plane perpendicular to the $[1\bar{1}0]$ direction is retained as a symmetry element. However, the results again do not favor the presence of ordered alloy layers, e.g., the following combination: (Pd+Pt) in the topmost layer, 2Pt in the second layer, (Pd+Pt) in the third layer, and 2Pd in the fourth layer yields an *r* factor of 0.56, with partial *r* factors of 0.44 and 0.72 for integral and half-order beams, respectively.

Thus, we conclude that the missing-row model with second-layer row pairing and third-layer rumpling best describes the (1×2) structure of Pt on Pd(110). Three layers of Pt are present in the reconstructed phase, which corresponds to an ideal coverage of 2.5 ML. Optimum structural parameters and the minimum *r* factor are as follows: $d_{12} = 1.24$ Å, $d_{23} = 1.26$ Å, $d_{34} = 1.27$ Å, $d_{45} = 1.40$ Å, $\sigma = 0.06$ Å, $\delta = -0.23$ Å, and $r_P = 0.32$. In the same manner as for bulk Pt(110)-(1×2),[2,3] pairing occurs toward the missing row and the upper atom of the corrugated layer is directly beneath the missing row. The directions of these displacive movements are consistent with reducing the large corrugation of the missing-row reconstruction. Differences in the interlayer spacings relative to the truncated substrate geometry are as follows: $\Delta d_{12} = -9.5\%$, $\Delta d_{23} = -8.0\%$, $\Delta d_{34} = -7.3\%$, and $\Delta d_{45} = 2.2\%$. Plots of r_P as a function of a single structural parameter, with all other parameters fixed near their optimum values, are shown in Fig. 8. Experimental and best-fit theoretical $I(E)$ curves are visually compared in Fig. 9.

The Pendry *r* factor obtained for the (1×2) structure is comparable to the value of 0.36 reported for bulk Pt(110)-(1×2).[3] Nevertheless, it is unlikely that the (1×2) phase forms a continuous overlayer. For instance, the coverage of the (1×1) film leading to the (1×2) structure upon annealing is 0.5 ML less than the ideal coverage of the (1×2) structure. This suggests that the (1×2) phase occurs as patches with limited spatial extent along the [001] direction—to be consistent with the LEED pattern—with perhaps (1×1) areas of either bare Pd or one-layer thick Pt in between. If such (1×2) patches do exist, they must cover a large fraction of the surface since comparable integral and half-order intensities are observed. Unfortunately, there is no simple way (if any) to include inhomogeneity in LEED calculations, although it

TABLE III. Results for (1×2) intermixing models. Structural parameters in the average *T*-matrix approximation (ATA) models are fixed at the values listed for model 11 in Table II. M+P+R is defined in Table II.

	% Pt				Optimum % Pt	Pendry *r* factor		
Model	layer 1	layer 2	layer 3	layer 4	in varied layer	Int.	Half	Tot.
14 ATA	Varied	100	100	0	88	0.29	0.35	0.32
15 ATA	100	Varied	100	0	100	0.30	0.35	0.32
16 ATA	100	100	Varied	0	100	0.30	0.35	0.32
17 ATA	100	100	100	Varied	0	0.30	0.35	0.32

	Upper	Optimum parameters (Å)						Pendry *r* factor		
Model	atom	d_{12}	d_{23}	d_{34}	d_{45}	σ	δ	Int.	Half	Tot.
18 M(Pt)+P(Pt)+R(alloy)	Pt	1.22	1.27	1.26	1.35	0.07	−0.23	0.37	0.52	0.44
19 M(Pt)+P(Pt)+R(alloy)	Pd	1.19	1.33	1.25	1.35	0.05	−0.21	0.43	0.55	0.48

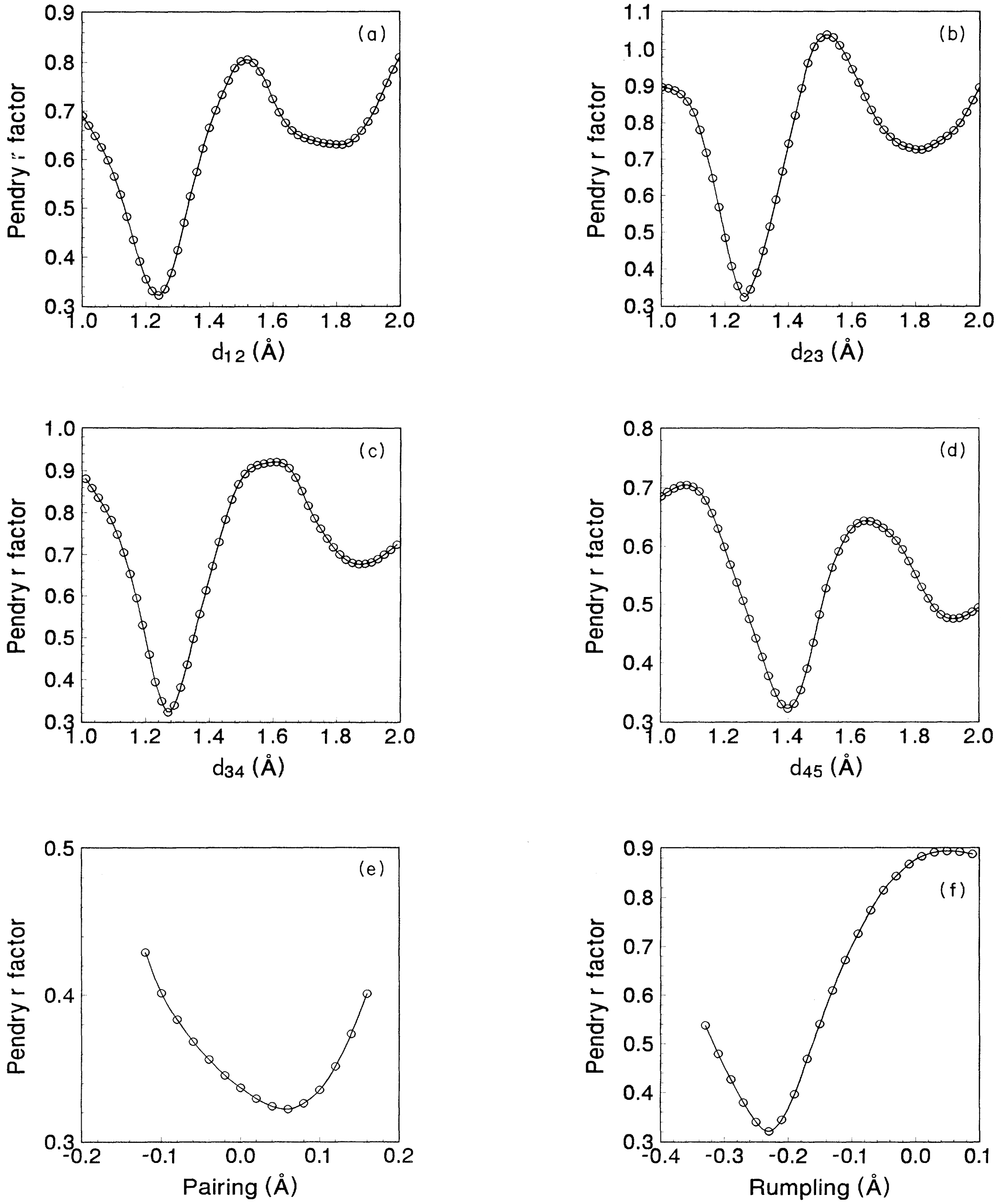

FIG. 8. Pendry r-factor sensitivity plots for the (1×2) structure. All parameters other than the parameter under consideration are fixed near their optimum values. (a) For d_{12}, (b) d_{23}, (c) d_{34}, (d) d_{45}, (e) pairing, and (f) rumpling.

TABLE IV. Comparison of Pt on Pd(110) results to Pt and Pd structures that have been determined by LEED.

Surface	Δd_{12} (%)	Δd_{23} (%)	σ (Å)	δ (Å)	Reference
Pd(110)-(1×2) (Cs-induced)	−9	−1	0.05	−0.1	34
Pt(110)-(1×2)	−18.4	−24.2	0.07	−0.32	2
Pt(110)-(1×2)	−20.9	−7.2	0.04	−0.17	3
Pt/Pd(110)-(1×2)	−9.5	−8.0	0.06	−0.23	this work
Pd(110)-(1×1)	−5.7	0.5			4
Pd(110)-(1×1)	−5.1	2.9			5
Pt/Pd(110)-(1×1) (1 ML)	−11.0	6.6			this work
Pt/Pd(110)-(1×1) (2 ML)	−6.6	4.4			this work

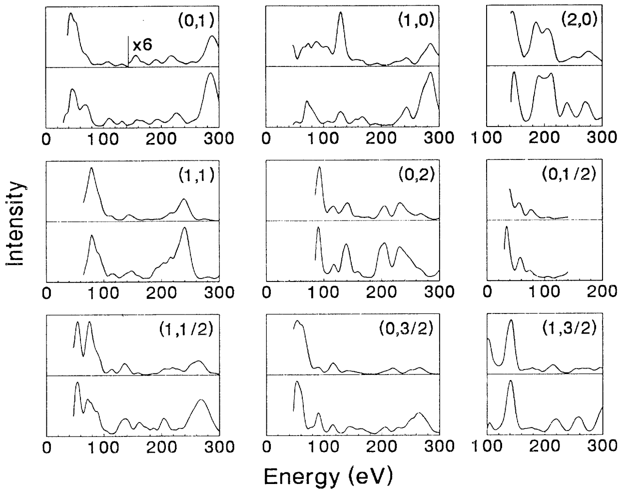

FIG. 9. Experimental and best-fit theoretical $I(E)$ curves for the (1×2) structure. Upper curves correspond to theory.

may be possible to improve the level of agreement by mixing in intensities from ordered (1×1) areas. However, such a procedure would not likely affect the final structure obtained for the (1×2) phase.

VI. DISCUSSION

A comparison with LEED results obtained for relevant surface structures of Pt and Pd is made in Table IV. While both (1×1) films are found to follow the trend of contracted d_{12} and expanded d_{23} characteristic of clean surfaces of bulk fcc(110)-(1×1) metals,[36] the magnitudes of the relaxations are found to depend on Pt coverage. The much larger contraction in d_{12} of the 1-ML film relative to that of either the 2-ML film or the clean substrate suggests that an attractive electronic interaction between Pt and Pd is present at the interface, i.e., bonding between Pt and Pd is stronger than either to itself. However, the attractive interaction does not appear to be strong enough to override the driving force for oscillatory relaxation when a second layer of Pt is present since this structure exhibits an expanded interlayer spacing at the interface.

It is known that strong bonding between the overlayer and substrate favors complete wetting for the first monolayer of deposition.[37] Therefore, it is reasonable to conclude that the (1×1) structure should be more stable than the missing-row-type structure at 1 ML since the (1×1) structure maximizes the number of Pt atoms in contact with the Pd substrate. Thus, it is not surprising that a minimum Pt coverage is required before reconstruction can set in. As mentioned previously, no evidence for superstructure formation is observed at Pt coverages ≤ 1 ML. The presence of an attractive electronic interaction is also consistent with a tendency to alloy,[37] which is supported by our observation of extensive film dissolution upon annealing to a sufficiently high temperature.

The optimum geometry of the (1×2) structure is found to be qualitatively similar to that of bulk Pt(110)-(1×2). Quantitatively, the most striking difference is that d_{12} of the Pt film is clearly found to be only half as contracted. Two factors could contribute to this difference. First, a lattice compression of 0.8% in the Pt overlayer—induced by the smaller surface unit cell of the Pd substrate—may create sufficient strain energy that a less contracted d_{12} results. Second, the relaxation of the (1×2) structure may be governed to some extent by the electronic influence of the Pd substrate.

For clean surfaces of bulk fcc(110) metals, the reduction in total energy by reconstructing to the (1×2) missing-row-type structure is probably rather small since this phenomenon occurs only for Pt, Au,[38] and Ir.[39] In fact, a first-principles calculation has shown that the surface energy of the (1×2) phase of Au is only ca. 5% lower than that of the (1×1) phase.[40] Further evidence for a small difference in the stability of the two phases is that clean surfaces of bulk fcc(110)-(1×1) metals can be pushed into the (1×2) missing-row-type structure by a slight disturbance, e.g., by a small fraction of a monolayer of alkali metal.[34] Thus, subtle modifications in the electronic structure of fcc(110) metals can cause significant changes in geometric structure. Based on these arguments, a less contracted d_{12} due in part to a different electronic environment is understandable.

ACKNOWLEDGMENTS

The experimental component of this work is supported primarily by the National Science Foundation through Grant No. CHE-9014214, and by the Ford Motor Company. R. J. Baird and G. W. Graham of Ford Motor Company are thanked for the use of their Pd(110) crystal. M. A. Van Hove is thanked for supplying LEED programs and phase shifts for the (1×1) analysis. E. Arola is thanked for providing the Pt potential for the (1×2) analysis. One of us (O.L.W.) acknowledges the support of the Amoco Foundation, and another (P.J.S.) acknowledges the support of Phillips Petroleum. P.A.T. acknowledges support from NSF Grant No. CHE 90 24358 and the Camille and Henry Dreyfus Foundation. Some equipment and all facilities are provided by the Ames Laboratory, which is operated for the U.S. Department of Energy by Iowa State University under Contract No. W-7405-ENG-82.

---

[*] Present address: Department of Chemistry, National University of Singapore, Singapore 05011.

[†] Present address: Ford Motor Company, Dearborn, MI 48121.

[1] P. Fenter and T. Gustafsson, Phys. Rev. B **38**, 10 197 (1988).

[2] E. C. Sowa, M. A. Van Hove, and D. L. Adams, Surf. Sci. **199**, 174 (1988).

[3] P. Fery, W. Moritz, and D. Wolf, Phys. Rev. B **38**, 7275 (1988).

[4] R. D. Diehl, M. Lindroos, A. Kearsley, C. J. Barnes, and D. A. King, J. Phys. C **18**, 4069 (1985).

[5] M. Skottke, R. J. Behm, G. Ertl, V. Penka, and W. Moritz, J.

Chem. Phys. **87**, 6191 (1987).

[6]M. Wolf, A. Goschnick, J. Loboda-Cacković, M. Grunze, W. N. Unertl, and J. H. Block, Surf. Sci. **182**, 489 (1987).

[7]C. Kittel, *Introduction to Solid State Physics* (Wiley, New York, 1976).

[8]J. H. van der Merwe, Philos. Mag. A **45**, 127 (1982).

[9]W.-Y. Leung, P. J. Schmitz, H. C. Kang, and P. A. Thiel, Surf. Sci. **257**, 79 (1991).

[10]P. J. Schmitz, W.-Y. Leung, H. C. Kang, and P. A. Thiel, Phys. Rev. B **44**, 13 734 (1991).

[11]R. P. Elliot and F. A. Shunk, Bull. Alloy Phase Diagrams **2**, 482 (1982).

[12]T. Gritsch, D. Coulman, R. J. Behm, and G. Ertl, Phys. Rev. Lett. **63**, 1086 (1989), and references therein.

[13]J. Goschnick, M. Wolf, M. Grunze, W. N. Unertl, J. H. Block, and J. Loboda-Cacković, Surf. Sci. **178**, 831 (1986).

[14]G. E. Rhead, M.-G. Barthes, and C. Argile, Thin Solid Films **82**, 201 (1981).

[15]D. K. Flynn, W.-D. Wang, S.-L. Chang, M. C. Tringides, and P. A. Thiel, Langmuir **4**, 1096 (1988).

[16]J. R. Noonan and H. L. Davis, in *Determination of Surface Structure by LEED,* edited by P. M. Marcus and F. Jona (Plenum, New York, 1984).

[17]M. A. Van Hove and S. Y. Tong, *Surface Crystallography by LEED* (Springer, Berlin, 1979).

[18]R. Baudoing, Y. Gauthier, M. Lundberg, and J. Rundgren, J. Phys. C **19**, 2825 (1986).

[19]S. Crampin and P. J. Rous, Surf. Sci. **244**, L137 (1991).

[20]V. Moruzzi, J. Janak, and A. Williams, *Calculated Electronic Properties of Metals* (Pergamon, New York, 1978).

[21]Attributed to S. W. Wang.

[22]L. F. Mattheiss, Phys. Rev. **133**, A1399 (1964).

[23]H. B. Nielsen and D. L. Adams, J. Phys. C **15**, 615 (1982).

[24]J. B. Pendry, J. Phys. C **13**, 937 (1980).

[25]J. Quinn, Y. S. Li, H. Li, D. Tian, F. Jona, and P. M. Marcus, Phys. Rev. B **43**, 3959 (1991).

[26]M. L. Xu and S. Y. Tong, Phys. Rev. B **31**, 6332 (1985).

[27]K. P. Bohnen, C. T. Chan, and K. M. Ho, Surf. Sci. **268**, L284 (1992).

[28]D. F. Ogletree, M. A. Van Hove, and G. A. Somorjai, Surf. Sci. **173**, 351 (1986).

[29]M. Henzler, Surf. Sci. **22**, 12 (1970).

[30]E. Zanazzi, F. Jona, D. W. Jepsen, and P. M. Marcus, J. Phys. C **10**, 375 (1977).

[31]D. K. Flynn, J. W. Evans, and P. A. Thiel, J. Vac. Sci. Technol. A **7**, 2162 (1989).

[32]J. W. Evans, D. E. Sanders, P. A. Thiel, and A. E. DePristo, Phys. Rev. B **41**, 5410 (1990).

[33]H. P. Bonzel and S. Ferrer, Surf. Sci. **118**, L263 (1982).

[34]C. J. Barnes, M. Lindroos, and D. A. King, Surf. Sci. **201**, 108 (1988).

[35]D. L. Adams, H. B. Nielsen, M. A. Van Hove, and A. Ignatiev, Surf. Sci. **104**, 47 (1981).

[36]For examples, see J. M. MacLaren, J. B. Pendry, P. J. Rous, D. K. Saldin, G. A. Somorjai, M. A. Van Hove, and D. D. Vvedensky, *Surface Crystallographic Information Service* (Reidel, Boston, 1987).

[37]J. H. van der Merwe, in *Chemistry and Physics of Solid Surfaces 5*, edited by R. Vanselow and R. Howe (Springer, Berlin, 1984).

[38]W. Moritz and D. Wolf, Surf. Sci. **163**, L655 (1985).

[39]C.-M. Chan and M. A. Van Hove, Surf. Sci. **171**, 226 (1986).

[40]K.-M. Ho and K. P. Bohnen, Phys. Rev. Lett. **59**, 1833 (1987).

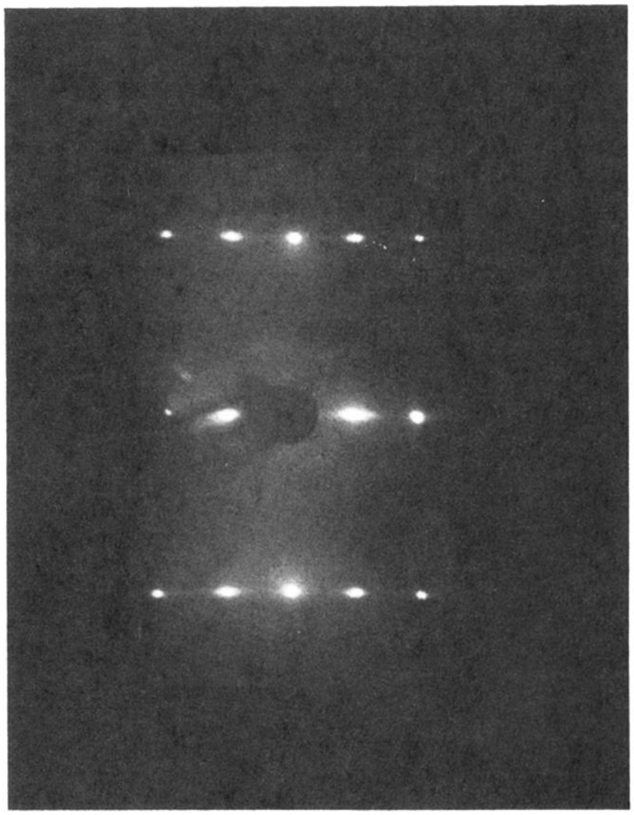

FIG. 2. (1×2) LEED pattern at 70 eV. $(0,\frac{1}{2})$, (0,1), (1,0), $(1,\frac{1}{2})$, and (1,1) beam sets are visible. Note the elongation of the half-order beams along the [001] direction.